 doi:10.20944/preprints202101.0119.v1

Aritcle

VEGF Detection via Simplified FLISA using a 3D Microfluidic Disk Platform

Dong Hee Kang [1], Na Kyong Kim [1], Sang-Woo Park [2,*] and Hyun Wook Kang [1,*]

[1] Department of Mechanical Engineering, Chonnam National University, 77 Yongbong-ro, Buk-gu, Gwangju 61186, Republic of Korea; (D.H.K) kdh05010@gmail.com; (N.K.K) naky0607@gmail.com

[2] Department of Ophthalmology, Chonnam National University Medical School and Hospital, Baekseo-ro, Dong-gu, Gwangju 61469, Republic of Korea

* Co-Correspondence: (H.W.K) kanghw@chonnam.ac.kr; Tel.: +82-62-530-1662; (S.W.P) exo70@naver.com

Abstract: Fluorescence-linked immunosorbent assay (FLISA) is a commonly used, quantitative technique for detecting biochemical based on antigen–antibody binding reactions using a well-plate platform. With the developments in the manufacturing technology of microfluidic systems, FLISA can be implemented onto microfluidic disk platforms, which allows the detection of trace biochemical with high resolutions. Apart from requiring a lower proportion of reagent (1/10), this method also reduces the time required for the entire process to less than an hour. The incubation process involves antigen–antibody binding reactions as well as the binding of fluorogenic substrates to target proteins. The protocol for FLISA on a microfluidic platform necessitates the appropriate execution of liquid reagent movements during each step in order to ensure sufficient binding reactions. Herein, we propose a novel microfluidic disk comprising a 3D incubation chamber. Vascular endothelial growth factor as concentration with ng mL^{-1} is detected sequentially using a benchtop process employing this 3D microfluidic disk. The 3D microfluidic disk is implemented without requiring manual intervention or additional procedures for liquid control. During the incubation process, microbead movement is controlled through centrifugal force, generated due to disk rotation, and gravitational force via bead sedimentation on the sloped floor of the chamber.

Keywords: Lab-on-a-disk; 3D microstructure; FLISA; VEGF

1. Introduction

Owing to recent technological and medical developments, the average life expectancy of humans has increased; this, in turn, has significantly increased the incidence of age-related ocular diseases. A recent study reported that the increase in the prevalence rate of ocular diseases is strongly correlated with higher concentrations of vascular endothelial growth factor (VEGF). [1-6] Several ocular diseases associated with the concentration of VEGF, such as proliferative diabetic retinopathy [7], ocular ischemic syndrome [8], and retinal vein occlusions [9], can cause retinal ischemia, which can result in devastating changes on the function and anatomy of ocular structures. Increased VEGF in the vitreous and aqueous humor is the pathognomonic finding in most ischemic eye disease and thus the monitoring of the change of VEGF can be indispensable for predicting the treatment effectiveness and prognoses of such diseases. [10-13] However, the low concentration of VEGF and limited collecting of aqueous humor make it difficult to measure the change of VEGF in clinical practice.

Fluorescence-linked immunosorbent assay (FLISA) is a plate-based technique for quantifying trace-level proteins, even in concentrations of picograms per milliliter. [14-17] The FLISA protocol for using a micro-well plate platform requires more than 100 μL of the sample in order to detect protein with pg mL^{-1} levels. Considering the change in intraocular pressure, the amount of aqueous humor that can be extracted for VEGF measurements is limited to 50–100 μL. [18,19] Moreover, in general,

Preprints (www.preprints.org) | NOT PEER-REVIEWED | Posted: 6 January 2021 doi:10.20944/preprints202101.0119.v1

two or more incubation steps in the FLISA protocol require 1–2 hr each for the binding reaction between proteins. [20-23] Furthermore, repeated washing between these incubation steps is necessary to remove the remaining reagents. Therefore, the FLISA protocol is a time-consuming and complicated assay procedure. Consequently, innovations in microliter-scaled sample diagnostics are necessary for fast and high-accuracy measurements requiring small samples.

In several studies focusing on FLISA-based biochemical detection in lab-on-a-disk platforms, the total protocol execution time could be significantly reduced to under 1 hr by using microbeads. [24-30] Lee *et al*. presented a fully automated immunoassay using whole blood on a disk platform; this entire process was completed within 0.5 hr through a fully automated disk-based bioassay for infectious disease (antibody of Hepatitis B) detection. [29] Walsh *et al*. reported that fluorescence intensity results with a resolution of 1 ng mL^{-1} could be obtained even if all reagents are simultaneously loaded into the chamber, using an incubation process requiring 10 min. A simplification of the FLISA protocol helps improve the efficiency of quantitative analyses. [18] These results indicate that bead-based FLISA can reduce the protocol time due to the high specific volume of binding reagents. This is an advantage of microfluidic platforms, because they only require one-tenth of the reagent volume used in conventional plate-based FLISA. Moreover, the washing and detection processes are sequentially controlled through bead sedimentation using the density difference under the centrifugal force acting on the disk, without requiring manual intervention. However, implementing the FLISA protocol on microfluidic disk-based platforms requires precise control as well as a reduction in the reagent volumes. Furthermore, the microfluidic system is subdivided for precise fluid control at each step of FLISA, thereby increasing the complexity and manufacturing costs. Poly(methyl methacrylate) (PMMA) sheets are frequently used for the low-cost manufacturing of microfluidic chips, because they enable the fabrication of thin and transparent chips. [31-34] However, PMMA sheet processing is inadequate for fabricating the complex microfluidic channel geometries required to apply the one-step incubation process to the FLISA protocol.

Recent studies on bead-based immunosorbent assays for protein detection have employed wax valve components for the sequential control of fluids and the bi-directional rotation control required to ensure sufficient mixing. [29, 35] During the incubation process, such wax valve components in the disk would surely isolate the chamber in order to block the inflow of other micro-liquids between the antigens and antibodies. To build a fully automated detection system, the microfluidic disks require a more complicated manufacturing process, which increases the unit cost.

In this regard, this study proposes a one-step process for the bead-based FLISA protocol for VEGF detection; this proposed method only employs the centrifugal force acting on a multi-material 3D microfluidic disk platform. This multi-material 3D microfluidic disk features a hybrid structure comprising laser-cut PMMA layers and a 3D-printed chamber layer. The 3D-printed block includes an incubation chamber with a sloped floor for controlling the mixing of reagents through the cyclic movement of beads. Moreover, the bead washing and fluorescence detection processes are performed without requiring any manual intervention or additional processes. Moreover, in this proposed design, only the incubation chamber, which requires precise microfluidic control in the microfluidic disk structure, was manufactured via 3D printing. Therefore, the proposed method is expected to reduce the overall cost of manufacturing microfluidic disks.

2. Results

2.1 Assembly of the 3D microfluidic disk

The 3D microfluidic disk is assembled in a layer-by-layer manner; laser-cut PMMA disk layers are sequentially stacked along with the 3D-printed block, as shown in figure. 1(a). The microchannel and washing chamber are fabricated by adopting pressure-sensitive adhesive (PSA) films between the seven laser-cut PMMA sheets. Laser cutting (Nova24 Laser Engraver; Thunder Laser) was used to process the PSA film-attached PMMA sheets into the shape of a disk. The PSA film-attached PMMA disk layers are then stacked sequentially, starting from the bottom cover layer up to the top cover layer. These layers are combined using pillars passing through the 5-mm holes on the disk

Preprints (www.preprints.org) | NOT PEER-REVIEWED | Posted: 6 January 2021 doi:10.20944/preprints202101.0119.v1

layers to ensure appropriate alignment. After assembling the 3D microfluidic disk, a press machine is used to apply a pressure of 4 MPa on the PSA films between the PMMA disk layers and the 3D-printed block for 10 min at room temperature.

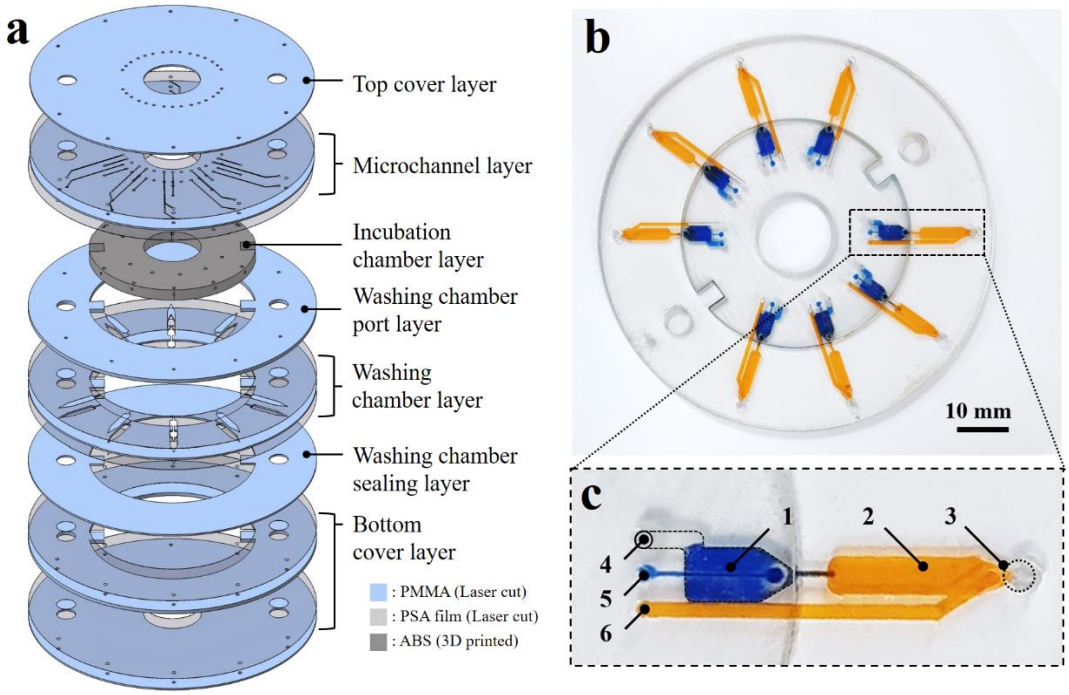

Figure 1. (a) Expanded view of the 3D microfluidic disk. (b) Image of the 3D microfluidic disk containing dyed water in the incubation (blue dye) and washing chambers (yellow dye). (c) Detailed view of the microfluidic module.

The PSA film prevents the leakage of liquid from the clearance between the PMMA layers and the 3D-printed block. The assembled 3D microfluidic disk, shown in figure. 1(b), features an incubation chamber (indicated by the blue-dyed water) and a washing chamber (indicated by the yellow-dyed water) that are connected through microchannels. Details of the microfluidic components in this 3D microfluidic disk are presented in figure. 1(c). The microfluidic circuit comprises the following components: (1) incubation chamber, (2) washing chamber, (3) fluorescence detection area, (4) vent of the incubation chamber, (5) inlet port of the incubation chamber, and (6) inlet port of the washing chamber. The incubation and washing chambers are connected through microchannels featuring rectangular cross-sections with widths of 300 ± 20 μm and 800 ± 20 μm, respectively. The height of the microchannel is 500 μm, which is also the thickness of the PMMA disk. The detection area at the end of the washing chamber has a sharp edge geometry. This detection area is covered with a transparent 500-μm PMMA disk in order to minimize excitation loss and emission light signal.

2.2. Simplified FLISA protocol

Immunological assays are commonly used techniques for the quantification of protein levels based on antibody–antigen interactions, using absorbent or fluorescent materials. Enzyme-linked immunosorbent assay (ELISA) is based on well-plate platforms; it employs enzymes that trigger a change in the color of the substrate. In this technique, the light absorption ratio is varied using the concentration of these enzymes. However, there are limitations when adopting this light absorption mechanism for the ELISA protocol in microfluidic systems. According to the Lambert–Beer law, the length of the path of light passing through the chamber with the reagent solutions directly affects the detection resolution. In particular, it is difficult to reduce the thickness of the disk in a microfluidic platform. Alternatively, FLISA can detect the superimposition of fluorescence intensities, even when using small sample volumes. The bead-based FLISA protocol for microfluidic disk platforms is particularly advantageous for the detection of fluorescence signals from aggregated fluorescence-

Preprints (www.preprints.org) | NOT PEER-REVIEWED | Posted: 6 January 2021 doi:10.20944/preprints202101.0119.v1

linked beads. This "simplified" FLISA protocol facilitates the incubation process and reduces the time required for antibody–antigen interactions. Moreover, the reagents are simultaneously loaded in to the incubation chamber, where they undergo mixing and are bound together. In this study, the reagents are prepared as depicted in figure. 2.

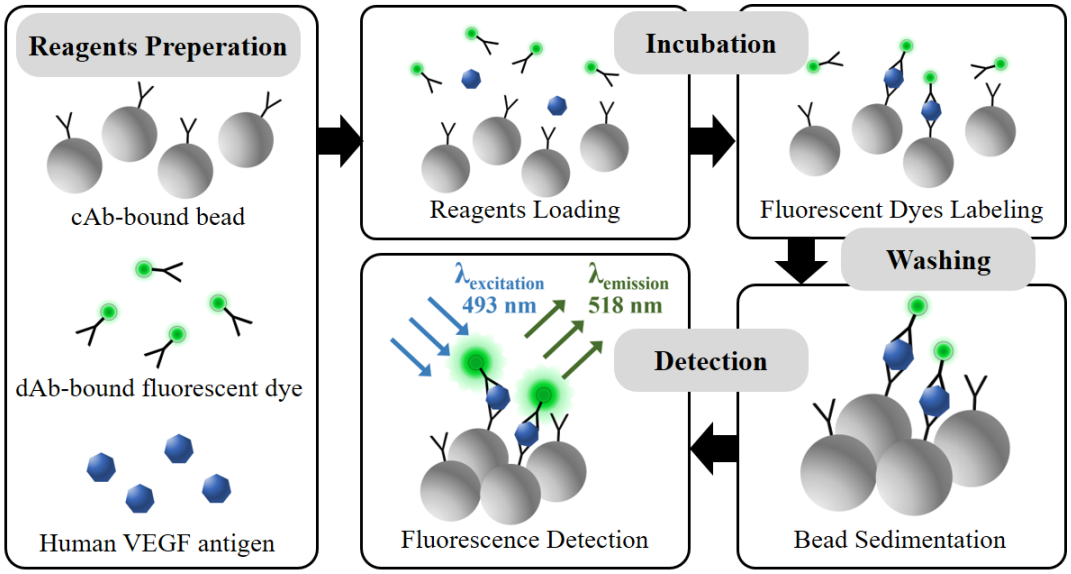

Figure 2. Schematic of the simplified bead-based FLISA protocol for VEGF detection. Bioassay between reagents is performed during incubation. The unbound dAb-fluorescent dye is removed via washing, along with bead sedimentation. The fluorescence signal is measured for VEGF detection.

Prior to applying the simplified bead-based FLISA to the microfluidic disk platform, this protocol is first implemented using a 96-well plate in order to ensure that the fluorescence signal intensities are linearly proportional to the reagent volumes and incubation times. The cAb-bound beads, human VEGF antigens, and dAb-bound fluorescent dye are simultaneously loaded into the micro-well with a volume ratio of 1:1:1. The well-plate is placed on a shaking incubator at 36°C and 120 rpm for 2 hr, during the incubation process. The beads are held at the bottom of the well-plate using a magnet. The unbound reagents are removed via washing with three times pipetting in the washing process. For the detection, a fluorescence microscope is used to confirm the amount of fluorescent dye-coupled beads that affect the fluorescence signal intensity with respect to VEGF concentration.

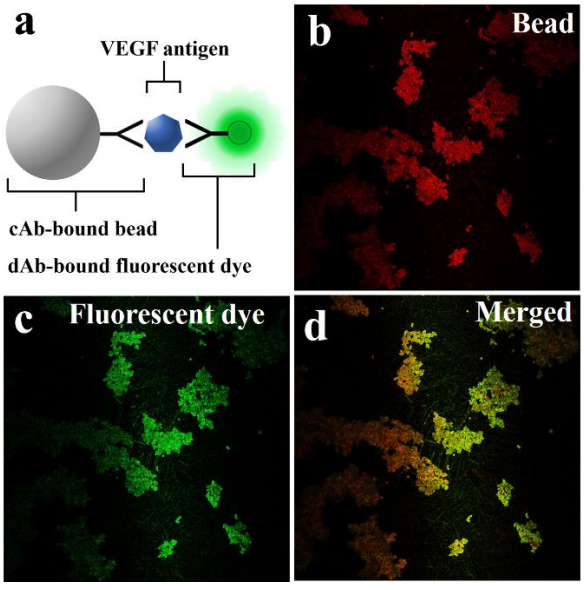

Preprints (www.preprints.org) | NOT PEER-REVIEWED | Posted: 6 January 2021 doi:10.20944/preprints202101.0119.v1

Figure 3. (a) Schematic of fluorescent dye-coupled VEGF on the beads. (b–d) Red, green, and merged fluorescence images for the fluorescent dye-coupled VEGF on the beads in the well-plate.

2.3. Characteristics of simplified bead-based FLISA protocol

The schematic in figure. 3(a) depicts the fluorescent dye-coupled bead surface formed via VEGF antigen–antibody affinity during the incubation process in FLISA. Figures. 3(b) and (c) present fluorescence microscopic images, where the red and green colors represent the beads and the fluorescent dye, respectively. The colocalized red and green fluorescence image, shown in figure. 3(d), represents the fluorescent dyes located in the same area as the beads. The simplified bead-based FLISA for VEGF detection, employing the 3D microfluidic disk platform, reduces the reagent volumes required and also decreases the incubation time. The fluorescence intensities for varying VEGF concentrations are compared. Moreover, to assess the performance of the simplified bead-based FLISA under variations in reagent volume and incubation time, the green fluorescence intensities are analyzed for VEGF concentrations of 1 μg mL^{-1} and 1 ng mL^{-1} as well as the pure PBS solution. In the simplified bead-based FLISA protocol, 100 μL of reagent (required for the conventional technique) is reduced to 10 and 5 μL, while the incubation time of 2 hr is reduced to 1 hr.

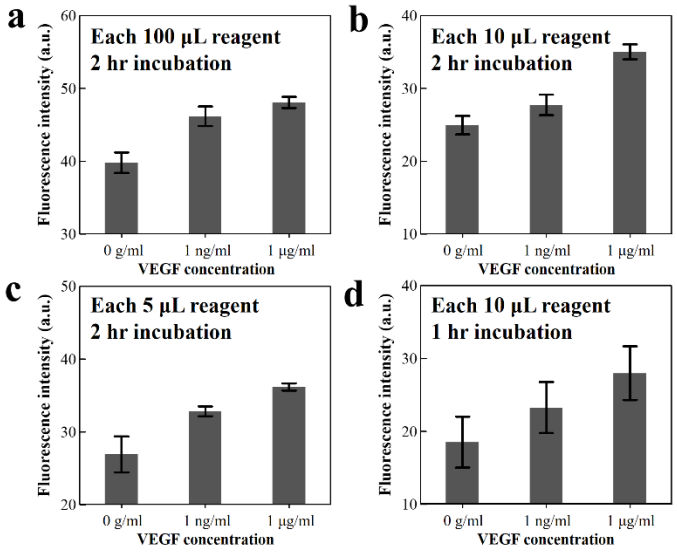

Figure 4. (a–c) Fluorescence intensity of the fluorescent dye-coupled VEGF on the beads after the 2 hr incubation, with reagent volumes of 100, 10, and 5 μL, respectively. (d) Fluorescence intensity of the fluorescent dye-coupled VEGF on the beads after the 1 hr incubation, with a reagent volume of 10 μL.

As shown in figure. 4, the fluorescence intensities are analyzed according to different VEGF concentrations, while maintaining the reagent volumes and incubation times. For the VEGF antigen solution with a concentration of 1 μg mL^{-1}, when using reagent volumes of 100, 10, and 5 μL, the fluorescence intensities are 48.08, 35.03, and 36.19, respectively. Moreover, for the same VEGF antigen solution with a concentration of 1 μg mL^{-1}, when using a reagent volume of 10 μL, the fluorescence intensity is reduced from 35.03 to 28.0 on decreasing the incubation time from 2 hr to 1 hr. Decreasing the reagent volume (from 100 to 10 μL) and the incubation time (from 2 hr to 1 hr) causes fluorescent intensity reductions of 34.8% and 20.5%, respectively. It can be concluded that the linearity of the detected fluorescence intensity is retained, even when using small reagent volumes and shorter incubation periods. Despite this reduction in reagent volume and incubation period, the results can be analyzed using image processing by increasing the resolution through background noise elimination and fluorescence signal amplification. Thus, the simplified bead-based FLISA employing a reagent volume of 10 μL and an incubation time of 1 hr is performed on the 3D microfluidic disk.

Preprints (www.preprints.org) | NOT PEER-REVIEWED | Posted: 6 January 2021 doi:10.20944/preprints202101.0119.v1

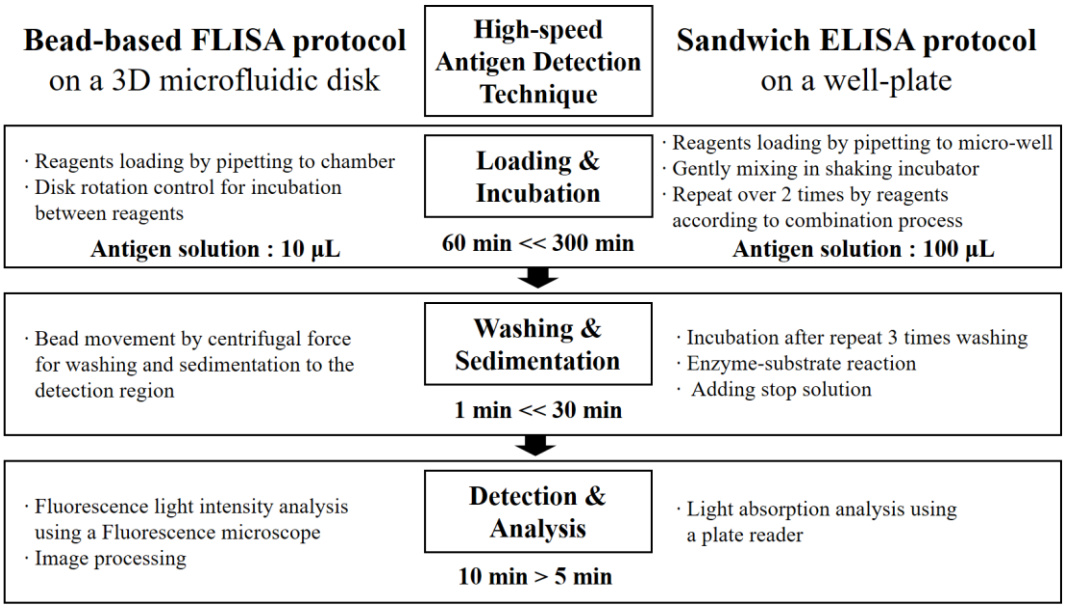

Figure 5. A flow chart to comparison of antigen detection techniques between bead-based FLISA and sandwich ELISA protocols.

The bead-based FLISA protocol shows the possibility of detecting VEGF level in the range of 0.1 ng mL^{-1}, which can be criteria in diagnosis for clinical signs. As shown in figure. 5, when compared with conventional antigen detection technology using a sandwich ELISA method, the bead-based FLISA protocol is possible to save as much as the required time for the incubation process and the volume of antigen solution to 1/5 and 1/10, respectively.

2.4. One-step simplified bead-based FLISA using 3D microfluidic disk

The simplified bead-based FLISA protocol using the 3D microfluidic disk is performed sequentially using a one-step process, involving reagent loading, incubation, washing, and detection.

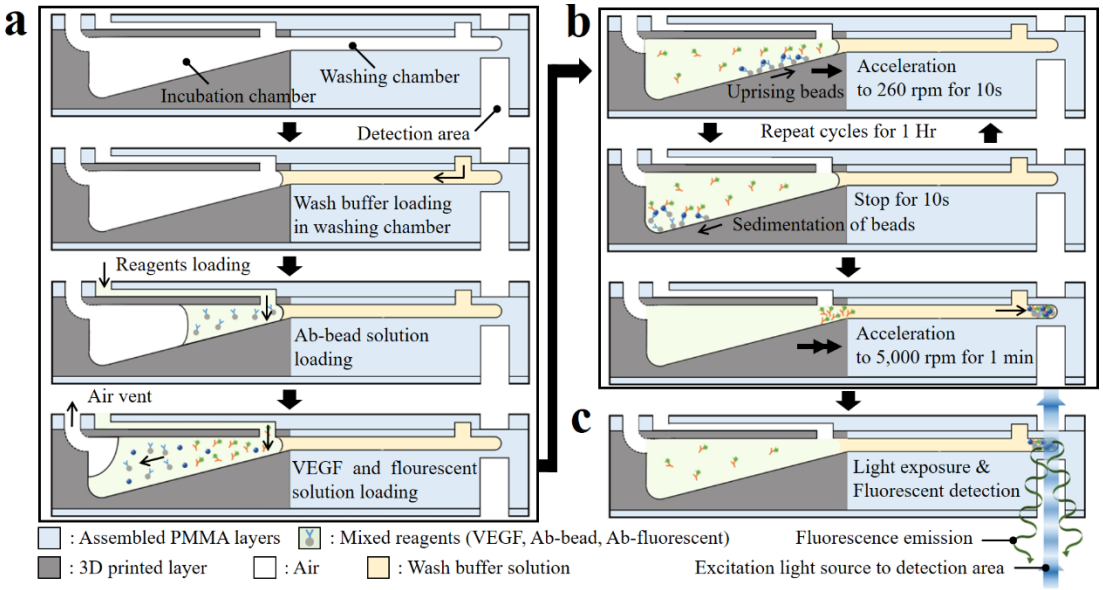

Figure 6. Schematic sectional view of the microfluidic module highlighting the sequential protocol of the simplified bead-based FLISA; the processes indicated are (a) loading the wash buffer solution and reagents, (b) incubation, and (c) fluorescence detection, respectively.

Figure. 6 present schematics of the cross-section of the microfluidic circuit along the radial direction of the disk in order to highlight the proposed sequential process. First, 30 µL of the wash buffer

Preprints (www.preprints.org) | NOT PEER-REVIEWED | Posted: 6 January 2021 doi:10.20944/preprints202101.0119.v1

solution is loaded into the washing chamber through the inlet port. The reagents cAb-bound bead solution, VEGF antigen solution, and dAb-bound fluorescent dye solution are sequentially loaded into the incubation chamber using pipettes; 10 μL of each reagent is used. After loading these reagents and the wash buffer in the 3D microfluidic disk, the disk is placed on a spindle motor located inside a darkroom to avoid the photobleaching of the fluorescent dye during the incubation process. The inlet ports are blocked using commercial transparent tape to prevent the evaporation of the reagents during the protocol. For the incubation process, disk rotation is regulated to ensure that the reagents are mixed sufficiently. In the incubation chamber with the sloped floor, beads move along the radial direction of the chamber, while accelerating at 260 rpm for 10 s. Subsequently, when disk rotation is stopped for 10 s, the beads on the slope move back to the center of the bottom of the chamber due to the slope and gravitational force. This movement of the beads is controlled by adjusting the centrifugal force in order to improve the mixing between reagents during incubation. The angular velocity of the disk affects the bead movement during sedimentation according to Stokes' law, which can be expressed as Eq. 1:

$$U_s = \frac{2}{9}\frac{(\rho_{bead} - \rho_f)}{\mu} aR^2 \quad (1)$$

Where U_s is the sedimentation velocity; ρ_{bead} and ρ_f are the bead and fluid densities, respectively; μ is the fluid viscosity; R is the radius of the beads; and a is the acceleration. Here, for the bead in the incubation chamber with a sloped floor, the acceleration is changed to $a \cdot cos\theta - g \cdot sin\theta$, where θ and g are the slope of the incubation chamber and gravitational acceleration, respectively. For the mixing cycle during incubation and the bead washing process, the angular velocity of the disk with respect to time is shown in figure. S1. In the incubation chamber, when the disk rotates at 260 rpm for one cycle and then stops for 10 s, the beads move by 5.50 ± 2.86 μm along the radial direction and then move back by 3.22 μm, according to Stokes' law (Eq. 1). When the disk is rotating, the distance traversed by the bead depends on its radial position relative to the central axis of the disk. For a stationary disk, the beads on the slope of the incubation chamber are only influenced by gravitational force and move toward the central axis, regardless of their position. The incubation between reagents is performed by means of gentle mixing for 1 hr. After this incubation process, the disk is accelerated to 5,000 rpm for 10 s and then washed for 1 min. The unbound dAb-fluorescent dye is separated due to the difference in density when the beads pass through the wash buffer solution. During this process, the fluorescent dye-coupled beads as well as the unlabeled beads settle together at the end of the washing chamber.

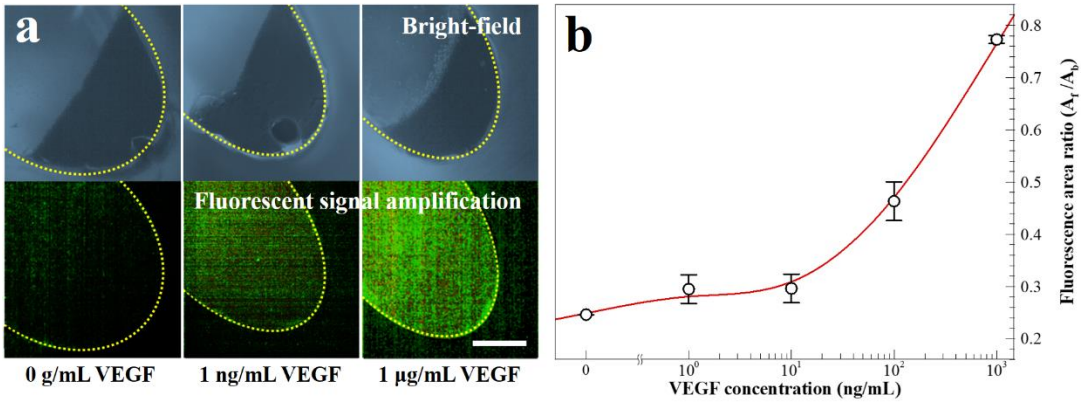

Figure 7. (a) Bright-field and fluorescence images for fluorescent dye-coupled beads, with VEGF concentrations of 0 g mL^{-1}, 1 ng mL^{-1}, and 1 μg mL^{-1}. (scale bar = 100 μm) (b) Fluorescence intensity with varying VEGF concentrations.

Figure. 7(a) presents the bright and fluorescent images indicating fluorescent dye-coupled beads with VEGF concentrations of 1 ng mL^{-1} and 1 μg mL^{-1} and the unlabeled beads at the end of the washing chamber. The yellow dotted line in this figure denotes the end of the washing chamber. The results of the fluorescence area ratio, A_f/A_b, are shown in figure. 7(b); this parameter is calculated using the

Preprints (www.preprints.org) | NOT PEER-REVIEWED | Posted: 6 January 2021 doi:10.20944/preprints202101.0119.v1

fluorescence area (A_f) and the bead-aggregated area (A_b). The value of A_f/A_b increases with the VEGF concentration between 1 μg mL^{-1} and 0 g mL^{-1}.

3. Discussion

To summarize, in this study, a simplified bead-based FLISA protocol is performed using a multi-material 3D microfluidic disk for VEGF detection. The proposed hybrid microfluidic disk structure comprises a 3D-printed block and laser-cut PMMA layers containing an incubation chamber and a washing chamber with microchannels, respectively. The activated PSA films between the 3D printed block and the PMMA layers maintain the disk structure, while preventing reagent leakage during the simplified bead-based FLISA protocol. In the proposed simplified FLISA protocol, the fluorescence signal intensity is linearly related to the VEGF concentration, regardless of reagent volume and variations in incubation time. In the 3D microfluidic disk, the entire simplified bead-based protocol can be completed within an hour without requiring additional manual intervention. Moreover, the fluorescence signals can be detected immediately after completing the rotation of the disk. The green fluorescent images thus obtained are analyzed using image processing software. As a result, VEGF detection can be achieved to ng mL^{-1} resolution using the A_f/A_b fluorescence area ratio analysis via a one-step simplified bead-based FLISA employing a 3D microfluidic disk. Furthermore, in order to improve detection resolution for target antigens as well as VEGF, cAb–bound bead movement can be precisely controlled by manipulating disk acceleration and cycles with bi-direction rotation.

4. Materials and Methods

4.1. Fabrication of 3D microfluidic disk and post treatment

The incubation chamber layer, which comprises eight independent incubation chambers, is first designed using a CATIA V5 software, which is a design and modeling program. The designed model is converted to the STL file format required for the 3D printing software. The incubation chamber layer is fabricated via stereolithography apparatus (SLA); 3D printing employing SLA enables the fabrication of micro structures with a roughness of ± 15 μm, as shown in figure. S2. The incubation chamber has a volume of 25 μL with a sloped floor. One side of the chamber is connected to a ventilation hole in the top layer of the block, and the other side of the chamber is connected to the side wall of the block for liquid transport; this configuration is presented in figure. S3. After 3D printing the block, post treatment is performed to remove the wax supports in the incubation chamber and to clean the surfaces. First, the supporting wax layers are roughly removed under a steam environment for 0.5 hr. Subsequently, the 3D-printed block is immersed in hot oil for 2 hr in order to completely remove the remaining wax in the chambers and the chamber walls. After cooling the block at room temperature for 10 min, ultrasonic cleaning with detergents and washing with deionized water were performed to remove the residual oil and clean the surfaces; each of these processes lasted for 10 min. Finally, this washed block is dried in a convection oven for 24 hr to eliminate the moisture in its microstructure. Also, microfluidic components in assembled 3D microfluidic disk are flushed to the remaining debris by pipetting 100 μL of phosphate buffer saline (PBS) solution (pH 7.4, Sigma-Aldrich) containing 0.5 wt% bovine serum albumin (BSA, Sigma-Aldrich) and once with 100 μL of distilled water. Thereafter, the 3D microfluidic disk is dried in a convection oven at room temperature for 24 hr.

4.2 Preparation of VEGF reagents

For reagent preparation, VEGF capture antibody (cAb) and VEGF detection antibody (dAb) are bound to bead surfaces and fluorescent dye, respectively. An antibody coupling kit (Dynabeads antibody coupling kit, Thermo Fisher) is used for binding the cAb (Human/Primate VEGF Antibody, R&D Systems) onto the surfaces of epoxy magnetic beads with a diameter of 2.8 μm (Dynabeads M-270 Epoxy, Thermo Fisher). This procedure requires 24 hr, according to the coupling protocol. The concentration of cAbs on the bead surfaces is 20 μg mg^{-1} in 1 mL of PBS solution containing 1 wt%

Preprints (www.preprints.org) | NOT PEER-REVIEWED | Posted: 6 January 2021 doi:10.20944/preprints202101.0119.v1

BSA. Furthermore, a fluorescence conjugation kit (DyLight 488 Conjugation kit, Abcam) is used for binding the fluorescent dye (DyLight 488) conjugation of dAb (Human VEGF 165 Antibody, R&D Systems) with a volume ratio of 1:1; these are then left overnight in the dark at room temperature. Subsequently, the dAb-bound fluorescent dye is diluted in PBS solution to a concentration of 1 μg mL^{-1}. Standard VEGF (Recombinant Human VEGF 165, R&D Systems) antigen solution is diluted using PBS with 10-fold serial dilution to 1 μg mL^{-1}, 100 ng mL^{-1}, 10 ng mL^{-1} and 1 ng mL^{-1}, and pure PBS without VEGF as the control solution. The wash buffer solution is prepared by adding 20 wt% dextran (Mr 15,000~25,000, Sigma-Aldrich) in PBST (PBS containing 0.05 % v/v Triton-X (Triton-X100, Sigma-Aldrich)) solution for 24 hr on a hot plate magnetic stirrer at 60°C.

4.3 Analysis and detection of fluorescence

A customized microscope is used for the measurement of fluorescence at the detection area in the 3D microfluidic disk; this microscope is located on the spindle motor, and fluorescence is measured immediately after completing the rotation. Fluorescence signals are measured in a darkroom to avoid light noise from the surroundings. The microscope employed a 150-W halogen fiber illuminator with optic filters. Optical filtration was used to selectively filter out fluorescence wavelengths using an excitation filter (473–491 nm at average light transmission (T_{avg}) > 93%), a dichroic filter (502–950 nm at T_{avg} > 93% and 350–488 nm at T_{avg} < 7%), and an emission filter (506–534 nm at T_{avg} > 93%). The microscopic images thus obtained are analyzed using ImageJ, an image processing software. Thus, within the border of the aggregated beads at the edge of the detection area, the fluorescence intensity is amplified, while the background noise is eliminated via high-pass filtration.

5. Conclusions

A simplified bead-based FLISA protocol using a 3D microfluidic disk composed of different materials is successfully conducted for the detection of VEGF. The 3D microfluidic disk comprises a 3D-printed block and PSA film-attached laser-cut PMMA layers. In the proposed protocol, only components requiring precise control are fabricated using 3D printing, whereas the remaining components are composed of PMMA disks in order to reduce the overall production cost. Moreover, microbeads are used as the substrate to apply the FLISA protocol using the microfluidic disk. The increased specific surface afforded by these microbeads facilitates antigen–antibody reactions, even for a reagent volume of 30 μL. Furthermore, in the simplified FLISA protocol, reagents are simultaneously loaded into the incubation chamber, and the reagent volumes can be reduced to 1/10, while maintaining the linearity of green fluorescence signals with respect to VEGF concentrations. The excited fluorescence signals observed during the detection process are superimposed from the aggregated beads at the edge of the detection area. High-resolution characteristics of the fluorescence area ratio, A_f/A_b, with respect to the VEGF concentration could be confirmed. Therefore, the 3D microfluidic disk platform can be used to detect VEGF on the sequential benchtop process using only passive mixing in simple clockwise rotation cycle within one hour. Regardless of the target antigen including VEGF, manipulating conditions of disk acceleration and cycles with bi-directional rotation enhances the physical contact opportunity to antigen-antibody interaction by microbead movement control. In the future, it can be applied in developing countries as a low-cost, ultra-high-speed diagnostic system for virus detection like COVID-19. This is possible to provide a platform for detecting biochemical targets within an hour by utilizing a 3D microfluidic disk and a simple rotor.

Supplementary Materials: Figure. S1. Angular velocity of disk with respect to time for the mixing cycle during incubation and the bead washing process. Figure. S2. SEM images of micropillars (designed diameter (D) =500, 250, 200, and 100 μm) on 3D printed surface fabricated in the (a–d) vertical and (e–h) lateral directions. Figure. S3. (a) Top view of 3D-printed block. (b) Isometric view and (c) sectional view of the 3D-printed block.

Author Contributions: Conceptualization, D.H.K., H.W.K. and S.W.P.; methodology, H.W.K. and S.W.P.; validation, N.K.K.; formal analysis, D.H.K. and N.K.K.; investigation, D.H.K., and S.W.P.; resources, H.W.K. and S.W.P.; writing—original draft preparation, D.H.K.; writing—review and editing, D.H.K., N.K.K., S.W.P. and

H.W.K.; supervision, S.W.P. and H.W.K.; project administration, S.W.P. and H.W.K.; funding acquisition, S.W.P. and H.W.K.

Funding: This research was supported by a grant from the Korea Health Technology R&D Project through the Korea Health Industry Development Institute (KHIDI), funded by the Ministry of Health & Welfare, Republic of Korea (grant number: HI19C0642), and funded by a grant (CRI18017-1) from Chonnam National University Hospital Biomedical Research Institute.

Conflicts of Interest: The authors declare no conflict of interest.

Abbreviations

BSA	Bovine Serum Albumin
cAb	Capture Antibody
dAb	Detection Antibody
ELISA	Enzyme-Linked Immunosorbent Assay
FLISA	Fluorescence-Linked Immunosorbent Assay
PMMA	Poly(methyl methacrylate)
PBS	Phosphate Buffer Saline
PBST	Phosphate Buffer Saline with Tween detergent
PSA	Pressure-Sensitive Adhesive
SLA	Stereo-Lithography Apparatus
VEGF	Vascular Endothelial Growth Factor

References

1. Ng, E. W.; Shima, D. T.; Calias, P.; Cunningham, E. T.; Guyer, D. R.; Adamis, A. P. Pegaptanib, a targeted anti-VEGF aptamer for ocular vascular disease. *Nat. Rev. Drug Discov.* **2006**, *5*, 123-132.
2. Witmer, A. N.; Vrensen, G. F. J. M.; Van Noorden, C. J. F.; Schlingemann, R. O. Vascular endothelial growth factors and angiogenesis in eye disease. *Prog.Retin. Eye Res.* **2003**, *22*, 1-29.
3. Nowak, J. Z. Age-related macular degeneration (AMD): pathogenesis and therapy. *Pharmacol. Rep.* **2006**, *58*, 353.
4. Lançon, A.; Frazzi, R.; Latruffe, N. Anti-oxidant, anti-inflammatory and anti-angiogenic properties of resveratrol in ocular diseases. *Molecules* **2016**, *21*, 304.
5. Penn, J. S.; Madan, A.; Caldwell, R. B.; Bartoli, M.; Caldwell, R. W.; Hartnett, M. E. Vascular endothelial growth factor in eye disease. *Prog.Retin. Eye Res.* **2008**, *27*, 331-371.
6. Schmidl, D.; Garhöfer, G.; Schmetterer, L. Nutritional supplements in age-related macular degeneration. *Acta ophthalmol.* **2015**, *93*, 105-121.
7. Gucciardo, E.; Loukovaara, S.; Salven, P.; Lehti, K. Lymphatic vascular structures: a new aspect in proliferative diabetic retinopathy. *Int. J. Mol. Sci.* **2018**, *19*, 4034.
8. Masuda, T.; Shimazawa, M.; Hara, H. The kallikrein system in retinal damage/protection. *Eur. J. Pharmacol.* **2015**, *749*, 161-163.
9. Wecker, T.; Ehlken, C.; Bühler, A.; Lange, C.; Agostini, H.; Böhringer, D.; Stahl, A. Five-year visual acuity outcomes and injection patterns in patients with pro-re-nata treatments for AMD, DME, RVO and myopic CNV. *Br. J. Ophthalmol.* **2017**, *101*, 353-359.
10. Eljarrat-Binstock, E.; Pe'er, J.; Domb, A. J. New techniques for drug delivery to the posterior eye segment. *Pharm. Res.* **2010**, *27*, 530-543.
11. Chang, J. H.; Garg, N. K.; Lunde, E.; Han, K. Y.; Jain, S.; Azar, D. T. Corneal neovascularization: an anti-VEGF therapy review. *Surv. Ophthalmol.* **2012**, *57*, 415-429.
12. Sulaiman, R. S.; Basavarajappa, H. D.; Corson, T. W. Natural product inhibitors of ocular angiogenesis. *Exp. Eye Res.* **2014**, *129*, 161-171.
13. Gupta, P.; Yadav, K. S. Applications of microneedles in delivering drugs for various ocular diseases. *Life Sci.* **2019**, *237*, 116907.
14. Zhang, C.; Han, Y.; Lin, L.; Deng, N.; Chen, B.; Liu, Y. Development of quantum dots-labeled antibody fluorescence immunoassays for the detection of morphine. *J. Agric. Food Chem.* **2017**, *65*, 1290-1295.

15. Lv, Y., Wu, R., Feng, K., Li, J., Mao, Q., Yuan, H., Shen, H.; Chai, X.; Li, L. S. Highly sensitive and accurate detection of C-reactive protein by CdSe/ZnS quantum dot-based fluorescence-linked immunosorbent assay. *J. Nanobiotechnol.* **2017**, *15*, 35.
16. Xiong, S.; Zhou, Y.; Huang, X.; Yu, R.; Lai, W.; Xiong, Y. Ultrasensitive direct competitive FLISA using highly luminescent quantum dot beads for tuning affinity of competing antigens to antibodies. *Anal. Chim. Acta* **2017**, *972*, 94-101.
17. Yao, J.; Xing, G.; Han, J.; Sun, Y.; Wang, F.; Deng, R.; Hu, X.; Zhang, G. Novel fluoroimmunoassays for detecting ochratoxin A using CdTe quantum dots. *J. Biophotonics* **2017**, *10*, 657-663.
18. Walsh III, D. I.; Sommer, G. J.; Schaff, U. Y.; Hahn, P. S.; Jaffe, G. J.; Murthy, S. K. A centrifugal fluidic immunoassay for ocular diagnostics with an enzymatically hydrolyzed fluorogenic substrate. *Lab Chip* **2014**, *14*, 2673-2680.
19. Hsu, M. Y.; Chen, S. J.; Chen, K. H.; Hung, Y. C.; Tsai, H. Y.; Cheng, C. M. Monitoring VEGF levels with low-volume sampling in major vision-threatening diseases: age-related macular degeneration and diabetic retinopathy. *Lab Chip* **2015**, *15*, 2357-2363.
20. Tabrizi, M. A., Shamsipur, M., Saber, R., Sarkar, S., & Ebrahimi, V. A high sensitive visible light-driven photoelectrochemical aptasensor for shrimp allergen tropomyosin detection using graphitic carbon nitride-TiO2 nanocomposite. *Biosens. Bioelectron.* **2017**, *98*, 113-118.
21. Jiang, S. H.; Li, J.; Dong, F. Y.; Yang, J. Y.; Liu, D. J.; Yang, X. M.; Wang, Y. H.; Yang, M.W.; Fu, X. L.; Zhang, X. X.; Li, Q.; Pang, X. F.; Huo, Y. M.; Li, J.; Zhang, J. F.; Lee, H. Y.; Lee, S. J.; Qin, W. X.; Gu, J. R.; Sun, Y. W.; Zhang, Z. G. Increased serotonin signaling contributes to the Warburg effect in pancreatic tumor cells under metabolic stress and promotes growth of pancreatic tumors in mice. Gastroenterology **2017**, *153*, 277-291.
22. Wu, Y.; Yi, L.; Li, E.; Li, Y.; Lu, Y.; Wang, P.; Zhou, H.; Liu, J.; Hu, Y.; Wang, D. Optimization of Glycyrrhiza polysaccharide liposome by response surface methodology and its immune activities. *Int. J. Biol. Macromol.* **2017**, *102*, 68-75.
23. Khang, H.; Cho, K.; Chong, S.; Lee, J. H. All-in-one dual-aptasensor capable of rapidly quantifying carcinoembryonic antigen. *Biosens. Bioelectron.* **2017**, *90*, 46-52.
24. Weiss, M.; Frohnmayer, J. P.; Benk, L. T.; Haller, B.; Janiesch, J. W.; Heitkamp, T.; Börsch, M.; Lira, R. B.; Dimova, R.; Lipowsky, R.; Bodenschatz, E.; Baret, J.; Vidakovic-Koch, T.; Sundmacher, K.; Platzman, I.; Spatz, J. P. Sequential bottom-up assembly of mechanically stabilized synthetic cells by microfluidics. *Nat. Mater.* **2018**, *17*, 89-96.
25. Barani, A.; Paktinat, H.; Janmaleki, M.; Mohammadi, A.; Mosaddegh, P.; Fadaei-Tehrani, A.; Sanati-Nezhad, A. Microfluidic integrated acoustic waving for manipulation of cells and molecules. *Biosens. Bioelectron.* **2016**, *85*, 714-725.
26. Miller, H.; Zhou, Z.; Shepherd, J.; Wollman, A. J.; Leake, M. C. Single-molecule techniques in biophysics: a review of the progress in methods and applications. *Rep. Prog. Phys.* **2017**, *81*, 024601.
27. Zhang, Y. N.; Zhao, Y.; Zhou, T.; Wu, Q. Applications and developments of on-chip biochemical sensors based on optofluidic photonic crystal cavities. *Lab Chip* **2018**, *18*, 57-74.
28. Ye, D.; Li, L.; Li, Z.; Zhang, Y.; Li, M.; Shi, J.; Zuo, X. Molecular threading-dependent mass transport in paper origami for single-step electrochemical DNA sensors. *Nano Lett.* **2018**, *19*, 369-374.
29. Lee, B. S.; Lee, J. N.; Park, J. M.; Lee, J. G.; Kim, S.; Cho, Y. K.; Ko, C. A fully automated immunoassay from whole blood on a disc. *Lab Chip* **2009**, *9*, 1548-1555.
30. Kang, D. H.; Kim, N. K.; Park, S. W.; Lee, W.; Kang, H. W. A microfluidic circuit consisting of individualized components with a 3D slope valve for automation of sequential liquid control. *Lab Chip* **2020**, *20*, 4433-4441.
31. Pourmand, A.; Shaegh, S. A. M.; Ghavifekr, H. B.; Aghdam, E. N.; Dokmeci, M. R.; Khademhosseini, A.; Zhang, Y. S. Fabrication of whole-thermoplastic normally closed microvalve, micro check valve, and micropump. *Sens. Actuators B-Chem.* **2018**, *262*, 625-636.
32. Bressan, L. P.; Adamo, C. B.; Quero, R. F.; de Jesus, D. P.; da Silva, J. A. A simple procedure to produce FDM-based 3D-printed microfluidic devices with an integrated PMMA optical window. *Anal. Methods* **2019**, *11*, 1014-1020.
33. Wondimu, S. F.; von der Ecken, S.; Ahrens, R.; Freude, W.; Guber, A. E.; Koos, C. Integration of digital microfluidics with whispering-gallery mode sensors for label-free detection of biomolecules. *Lab Chip* **2017**, *17*, 1740-1748.

34. Matellan, C.; Armando, E. Cost-effective rapid prototyping and assembly of poly (methyl methacrylate) microfluidic devices. *Sci. Rep.* **2018**, *8*, 1-13.
35. Park, J. M.; Cho, Y. K.; Lee, B. S.; Lee, J. G.; Ko, C. Multifunctional microvalves control by optical illumination on nanoheaters and its application in centrifugal microfluidic devices. *Lab Chip* **2007**, *7*, 557-564.